Journal of Magnetic Resonance **144,** 129–133 (2000)
doi:10.1006/jmre.2000.2031, available online at http://www.idealibrary.com on IDEAL®

^{1}H NMR Relaxation Investigation of Inhibitors Interacting with *Torpedo californica* Acetylcholinesterase

Maurizio Delfini,* Raffaella Gianferri,* Veronica Dubbini,* Cesare Manetti,* Elena Gaggelli,† and Gianni Valensin†

**Department of Chemistry, University of Rome La Sapienza, P.le A.Moro, 00195 Rome, Italy; and*
†Department of Chemistry, University of Siena, Via A.Moro, 53100 Siena, Italy

Received September 23, 1999; revised January 11, 2000

Two naphthyridines interacting with *Torpedo californica* acetylcholinesterase (AChE) were investigated. ^{1}H NMR spectra were recorded and nonselective, selective, and double-selective spin–lattice relaxation rates were measured. The enhancement of selective relaxation rates could be titrated by different ligand concentrations at constant AChE (yielding 0.22 and 1.53 mM for the dissociation constants) and was providing evidence of a diverse mode of interaction. The double-selective relaxation rates were used to evaluate the motional correlation times of bound ligands at 34.9 and 36.5 ns at 300 K. Selective relaxation rates of bound inhibitors could be interpreted also in terms of dipole–dipole interactions with protons in the enzyme active site.

INTRODUCTION

Acetylcholinesterase (AChE) catalyzes the hydrolysis of the ester bond of acetylcholine, a critical reaction for the termination of impulses transmitted through cholinergic synapses. The enzyme monomer unit is a member of the α/β class of proteins with a 12-stranded mixed β-sheet surrounded by 14 α-helices (*1, 2*). The structure contains a narrow cavity (ca. 2 nm deep), the "active-site gorge," lined by 14 aromatic residues and a peripheral anionic site at or near the entrance to the gorge. Besides organophosphorus poisons and toxins, AChE is the major target for inhibitors considered candidates for the symptomatic treatment of Alzheimer's disease (*3–5*). Although not universally accepted (*6*), this represents the most useful relieving strategy tested so far. Tacrine (*7*) and E2020 (*8*) are the two approved drugs so far. The X-ray structures of AChE complexed by tacrine (*9*) or E2020 (*5*) as well as other inhibitors (*9–13*) have been obtained, wherefrom the inhibitor selectivity for AChE in comparison with butyryl cholinesterase (BChE) is interpreted in terms of the molecular lining inside the gorge. This may be important because the less toxic drug (E2020) displays a ca. 1000-fold greater affinity for human AChE than for human BChE, whereas tacrine has a similar affinity for the two enzymes (*14, 15*). The main difference consists in interactions with ^{84}W at the bottom of the gorge (both ligands), ^{330}F at the midpoint of the gorge (diverse orientation), and ^{279}W at the peripheral anionic site at the top of the gorge (only E2020).

The search for potent, selective, and possibly less toxic inhibitors of AChE has led to synthesis of tacrine analogues, such as naphthyridines (*16*). Here we present NMR data of two naphthyridines (Fig. 1) interacting with AChE that allow us to suggest a useful NMR method for testing the AChE inhibition process and to yield delineation of relevant chemical features for rational drug design.

MATERIALS AND METHODS

The two derivatives were a gift of Dr. M. R. Del Giudice (Laboratorio di Chimica del Farmaco, Istituto Superiore di Sanità, Rome, Italy) and had been synthesized as reported elsewhere (*16*). AChE from *Torpedo californica* was obtained from Sigma and used without further purification. Solutions were prepared in deuterium oxide 100% (Sigma) buffered at pH 7.2 (phosphate saline buffer) and carefully deoxygenated with a few freezing vacuum pumping thawing cycles immediately followed by sealing off the NMR tube.

All NMR experiments were carried out on a Bruker AM 500 spectrometer at the controlled temperature of 300 ± 1 K. Chemical shifts were referenced to internal [$^2H_4$]trimethylsilylpropanesulfonate.

Proton spin–lattice relaxation rates were measured with inversion recovery pulse sequences and calculated by exponential regression analysis of recovery curves of longitudinal magnetization components.

Single- and double-selective proton spin–lattice relaxation rates were measured with inversion recovery pulse sequences implemented with DANTE or double-DANTE sequences (*17, 18*). All relaxation rates were calculated in the initial rate approximation (*19*).

RESULTS AND DISCUSSION

All chemical shifts of both derivatives were concentration dependent as expected for self-stacking aromatic rings. The plots reported in Fig. 2 were fit by the equation (*20*)

$$\delta_{obs} = \delta_D + \frac{\sqrt{(\delta_D - \delta_0)[1 - (8K_D[N]) + 1]}}{4K_D[N]}, \qquad [1]$$

1090-7807/00 $35.00

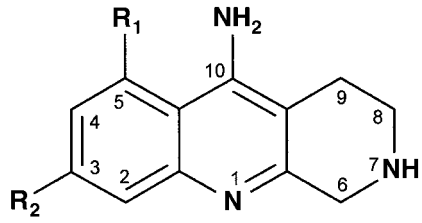

1a R_1 = H R_2 = Cl *10-amino-3-chloro-6,7,8,9-tetrahydro-[b][1,7]-naphtyridine*

1b R_1 = Cl R_2 = H *10-amino-5-chloro-6,7,8,9-tetrahydro-[b][1,7]-naphtyridine*

FIG. 1. (**1a**) R_1 = H, R_2 = Cl; 10-amino-3-chloro-6,7,8,9-tetrahydro-[1,7]-naphthyridine. (**1b**) R_1 = Cl, R_2 = H; 10-amino-5-chloro-6,7,8,9-tetrahydro-[1,7]-naphthyridine.

where δ_{obs} is the actual chemical shift measured at the concentration [N] of the naphthyridine, δ_D is the chemical shift of dimerized naphtyridine, δ_0 is the chemical shift of the monomer (i.e., at infinite dilution), and K_D is the dimerization constant. The fitting procedure yields the values of K_D for the self-aggregation constant at 2.1 and 2.5 M^{-1} for **1a** and **1b,** respectively. From these values it was inferred that at concentrations $\leq$1 mM the monomer is the predominant species in solution.

The proton relaxation rates, summarized in Table 1, were consistent with a relaxation mechanism mainly determined by

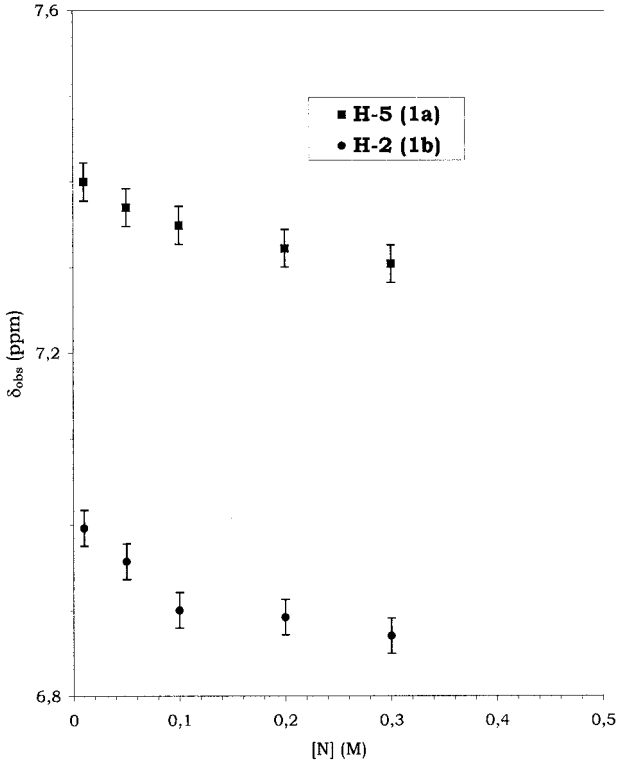

FIG. 2. Concentration dependence of ^{1}H NMR chemical shifts upon molar concentration for H_5 (**1a**) and H_2 (**1b**). T = 300 K.

TABLE 1
500-MHz ^{1}H NMR Parameters of 1 mM 1a and 1b in Deuterium Oxide at pH 7.2 and T = 300 K

1a Peak	δ (ppm)	R^{nsel} (s^{-1})	R^{sel} (s^{-1})	R^{nsel}/R^{sel}
H_4	7.87	0.649	0.414	1.568
H_2	7.61	0.294	0.226	1.301
H_5	7.41	0.469	0.368	1.274
H_6	4.25	2.336	1.600	1.460
H_8	3.46	2.237	2.155	1.038
H_9	2.77	2.273	2.247	1.012
1b Peak	δ (ppm)	R^{nsel} (s^{-1})	R^{sel} (s^{-1})	R^{nsel}/R^{sel}
H_4	7.87	0.269	0.269	1.000
H_2	7.56	0.282	0.264	1.068
H_5	7.42	0.523	0.484	1.081
H_6	4.30	2.533	1.736	1.459
H_8	3.48	2.028	2.092	0.969
H_9	2.88	1.984	2.012	0.986

^{1}H–^{1}H dipolar interactions as determined by the R^{nsel}/R^{sel} ratio (*19*). The motional correlation time was evaluated by the dipolar interaction energy between protons at fixed distances, σ^{ij}, as measured by double-selective relaxation rates according to the equation (*21*)

$$\sigma^{ij} = R_1^{ij} - R_i^{sel} = \frac{1}{10}\frac{\gamma^4\hbar^2}{r_{ij}^6}\left\{\frac{6\tau_{ij}}{1+\omega^2\tau_{ij}^2} - \tau_{ij}\right\}, \qquad [2]$$

where R_i^{ij} is the double-selective relaxation rate measured for H_i upon selective excitation of H_i and H_j, R_i^{sel} is the single-selective relaxation rate measured for H_i, γ is the proton magnetogyric ratio, $\hbar$ is the reduced Planck's constant ($\equiv h/2\pi$), r_{ij} is the H_i–H_j internuclear distance, ω is the proton Larmor frequency, and τ_{ij} is the motional correlation time characterizing reorientation of the H_i–H_j vector. Using this equation led us to evaluate the motional correlation time for **1a** at 92.8 $\pm$ 30.1 ps ($\sigma^{4,5}$ = 0.126 s^{-1}, $r_{4,5}$ = 0.243 nm) and that for **1b** at 42.5 $\pm$ 15.2 ps ($\sigma^{3,4}$ = 0.069 s^{-1}, $r_{3,4}$ = 0.243 nm), both at T = 300 K.

Upon addition of AChE up to a protein:ligand = 0.05 ratio, all chemical shifts were almost unaffected whereas all proton relaxation rates were selectively enhanced, R^{sel} being much more affected, as expected (*22–25*), than R^{nsel}. R^{nsel}/R^{sel} ratios were therefore consistently lowered. The enhancements of proton selective relaxation rates are shown in Fig. 3. In principle such effects might also be determined by the increased viscosity of the medium. However, as already noticed elsewhere (*22–25*), the fact that ΔR^{sel} is titratable by the ligand concentration at a fixed value of protein concentration (Fig. 4) demonstrates that the observed phenomena arise from binding to the protein with consequent slowing down of molecular motions. Moreover, occurrence of dipole–dipole interactions

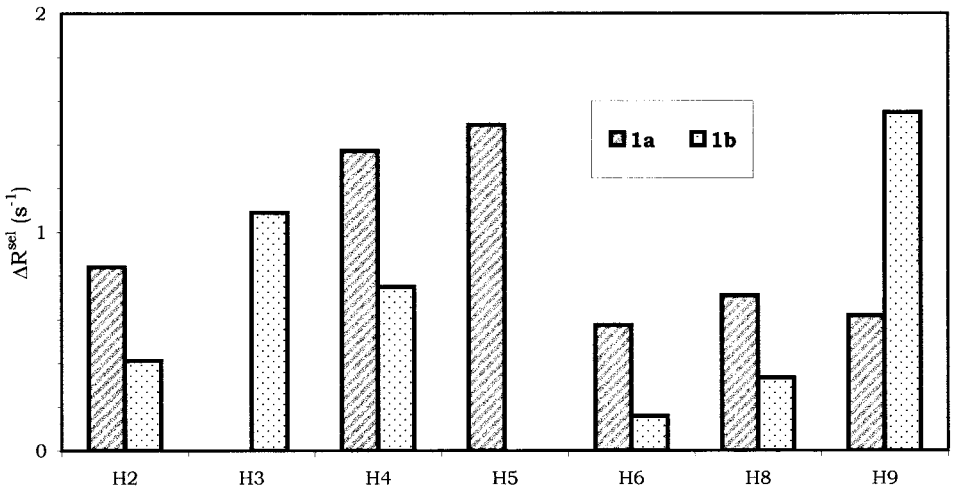

FIG. 3. Selective relaxation rate enhancements measured for 1 mM **1a** and **1b** in D_2O buffered at pH 7.2 in the presence of 5 μM *Torpedo californica* AChE. T = 300 K.

with protein protons is expected to contribute the relaxation rate enhancement.

Titration of ΔR^{sel} for affected protons (H_5 (**1a**) and H_2 (**1b**) are shown in Fig. 4) allows to evaluate the apparent dissociation constant by extrapolating data to $1/\Delta R^{sel} = 0$ where $[L] = -K_{diss}$ (*26*). The calculated values ($K_{diss} = 0.22 \pm 0.08$ mM for **1a** and $K_{diss} = 1.53 \pm 0.07$ mM for **1b**) suggest that the two inhibitors are differently bound by AChE, **1a** being much more tightly bound than **1b**. The proton relaxation time scale (≈ 1 s^{-1}) is such that the observed dissociation constants determine fast chemical exchange of the inhibitor between the protein-bound environment and the bulk such that relaxation rates measured in the presence of AChE are averaged according to the equations

$$R^{sel}_{obs} = p_{free}R^{sel}_{free} + p_{bound}R^{sel}_{bound} \quad [3a]$$

$$\sigma^{ij}_{obs} = p_{free}\sigma^{ij}_{free} + p_{bound}\sigma^{ij}_{bound}. \quad [3b]$$

The p fractions of ligand in each environment can be approximated by $p_{bound} = [\text{protein}]/[\text{ligand}]$, $p_{free} = 1 - p_{bound} \sim 1$. It follows that

$$R^{sel}_{obs} - R^{sel}_{free} = \Delta R^{sel} = p_{bound}R^{sel}_{bound} \quad [4a]$$

$$\sigma^{ij}_{obs} - \sigma^{ij}_{free} = \Delta\sigma^{ij} = p_{bound}\sigma^{ij}_{bound}. \quad [4b]$$

As a consequence the larger ΔR^{sel} is, the faster the corresponding selective relaxation rate is in the bound state. Such a rate is determined by reduced molecular motions accompanied by dipole–dipole interactions with protein protons. It is noticed that the aromatic ring of **1a** (H_4, H_5) and the aliphatic ring of **1b** (H_9) are the most affected, again suggesting a diverse mode of binding.

The cross-relaxation rates measured in the presence of AChE provide a means of improving the characterization of the binding interaction. Equation [4b] in fact allows for calculating

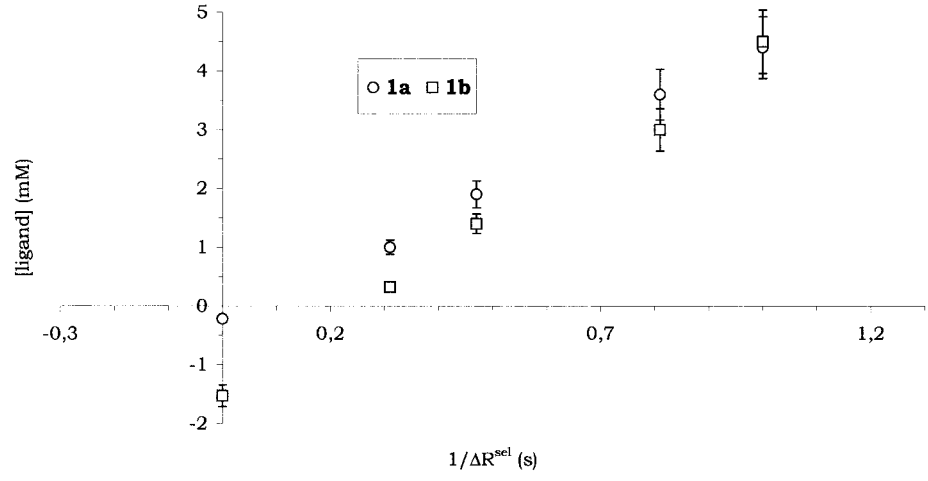

FIG. 4. Titration of selective relaxation rate enhancements for **1a** and **1b** in D_2O buffered at pH 7.2 in the presence of 5 μM *Torpedo californica* AChE. T = 300 K.

TABLE 2

Dipolar Interaction Energies Measured for Selected Proton Pairs of 1 mM 1a and 1b in D_2O Buffered at pH 7.2 in the Absence (σ^{ij}_{free}) and in the Presence (σ^{ij}_{obs}) of 5 μM *Torpedo californica* AChE, T = 300 K

	1a			1b		
Proton pair	σ^{ij}_{free} (s^{-1})	σ^{ij}_{obs} (s^{-1})	σ^{ij}_{bound} (s^{-1})	σ^{ij}_{free} (s^{-1})	σ^{ij}_{obs} (s^{-1})	σ^{ij}_{bound} (s^{-1})
H_8–H_9	0.019	−0.322	−6.82			
H_4–H_5	0.149	−0.334	−9.66			
H_8–H_9				0.020	−0.740	−15.21
H_3–H_4				0.070	−0.433	−10.12
H_2–H_3				0.068	−0.437	−10.04

the dipolar interaction energies of proton pairs in the bound state, as summarized in Table 2, where the σ^{ij} calculated in the presence of AChE are compared to those in the free solution state. The change from relatively small positive to large negative values is consistent with slowing down of molecular motions from a region where $\omega\tau \leq 1$ to one where $\omega\tau \gg 1$ (see Eq. [2]). The dipolar interaction energies in the bound state, σ^{ij}_{bound}, can be calculated by assuming $p_{bound} = 0.05 = [AChE]/[ligand]$ (see Eq. [4b]). Among the obtained values, those for the two H_8–H_9 proton pairs are not easily interpreted since the σ^{ij} is contributed by the H_8–H_8 (or H_9–H_9) geminal interaction and also by the four vicinal H_8–H_9 interactions. On the contrary the σ^{ij}_{bound} calculated for the H_4–H_5 and H_3–H_4 or H_2–H_3 proton pairs can be further handled for evaluating the motional correlation time of the two inhibitors in the binding pocket by considering $r_{4,5} = r_{3,4} = r_{2,3} = 0.243$ nm. Calculations (see Eq. [2]), provide $\tau_{4,5} = 34.9$ ns and $\tau_{3,4} = \tau_{2,3} = 36.5$ ns, both at T = 300 K, thus indicating that both inhibitors are tightly bound to the protein.

Single-selective proton spin–lattice relaxation rates of the inhibitor bound to AChE are very likely to be exclusively determined by a sum of direct relaxation rates extended to all pairwise interacting protons

$$R_i^{sel} = \sum_{j \neq i} \rho^{ij}, \qquad [5]$$

where

$$\rho^{ij} = \frac{1}{10} \frac{\gamma^4 \hbar^2}{r_{ij}^6} \left\{ \frac{3\tau_{ij}}{1 + \omega^2\tau_{ij}^2} + \frac{6\tau_{ij}}{1 + 4\omega^2\tau_{ij}^2} + \tau_{ij} \right\}. \qquad [6]$$

The evaluated correlation times are consistent with $\sigma^{ij} = -\rho^{ij}$ (see Eqs. [2] and [6]); this leads us to infer that the contribution of the H_4–H_5 interaction to R^{sel}_{bound} of H_5 in **1a** is 9.66 s^{-1}, while that of the H_3–H_4 interaction to R^{sel}_{bound} of H_3 in **1b** is 10.12 s^{-1}. These account for ca. 32 and 46% of the total R^{sel}_{bound} of H_5 (**1a**) and H_3 (**1b**), respectively, as calculated from Eq. [4a] with $p_{bound} = 0.05$. It can be therefore speculated that the aromatic ring of **1a** experiences a greater number of intermolecular interactions with protons of AChE when compared to the same ring of **1b**.

CONCLUSIONS

Since its very first applications, NMR has always attracted investigators of small molecules interacting with macromolecules. Besides the enormous and successful body of literature dedicated to paramagnetic systems, the NMR approach with unenriched samples has been always limited by the exchange rate from the bound state since only fast exchange yields sizeable changes in NMR parameters. Fast off-rates do not, of course, characterize the usual strong interactions with receptors, thus severely limiting NMR applications to systems of most biological relevance. AChE, on the contrary, with its extremely high catalytic efficiency, does allow NMR investigations of bound inhibitors, as demonstrated by the present data. Selective inhibitors, such as the two investigated naphthyridines, exchange from the bound state at a rate fast enough to yield measurable selective relaxation rate enhancements, thus providing relevant dynamic and structural features.

In the case of the two investigated inhibitors, the following properties were given evidence:

(i) the dissociation constant of **1a** is ca. one order of magnitude lower than that of **1b**;

(ii) the relaxation rates of aromatic ring protons of **1a** and aliphatic ring protons of **1b** are the most affected by addition of AChE;

(iii) the two inhibitors experience similar motional freedom in the 10-ns time scale;

(iv) intermolecular dipole–dipole interactions with protein protons are more effective in contributing relaxation rates of aromatic protons in **1a** than in **1b**.

All of these features, taken together, are consistent with a diverse orientation of the ligand within the active-site gorge; molecular models in fact show that a relatively small difference in the angle between the aromatic plane of the inhibitor and the main axis of the pocket may change the alignment of ^{330}F.

ACKNOWLEDGMENT

This work has been financed by Grant COFIN.MURST 97 CFSBI.

REFERENCES

1. J. L. Sussman, M. Harel, F. Frolow, C. Oefner, A. Goldman, L. Toker, and I. Silman, Atomic structure of acetylcholinesterase from *Torpedo californica:* A prototypic acetylcholine-binding protein, *Science* **253,** 872–879 (1991).
2. Y. Bourne, P. Taylor, P. E. Bougis, and P. Marchot, Crystal structure of mouse acetylcholinesterase, *J. Biol. Chem.* **274,** 2963–2970 (1999).
3. G. Pacheco, R. Palacios-Esquivel, and D. E. Moss, Cholinesterase inhibitors proposed for treating dementia in Alzheimer's disease:

Selectivity towards human brain acetylcholinesterase compared with butyrylcholinesterase, *J. Pharmacol. Exp. Ther.* **274,** 767–770 (1995).

4. S. C. Samuels and K. L. Davis, A risk–benefit assessment of tacrine in the treatment of Alzheimer's disease, *Drug Saf.* **16,** 66–77 (1997).
5. G. Kryger, I. Silman, and J. L. Sussman, Structure of acetylcholinesterase complexed with E2020 (Aricept): Implication for the design of new anti-Alzheimer drugs, *Structure* **7,** 297–307 (1999).
6. G. R. Swanwick and B. A. Lawlor, Initiating and monitoring cholinesterase inhibitor treatment for Alzheimer's disease, *Int. J. Geriatr. Psychiatry* **14,** 244–248 (1999).
7. K. L. Davis and P. Powchik, Tacrine. *Lancet* **345,** 625–630 (1995).
8. S. L. Nightingale, Donezipil approved for treatment of Alzheimer's disease, *J. Am. Med. Assoc.* **277,** 10 (1997).
9. M. Harel, I. Schalk, L. Ehret-Sabattier, F. Bouet, M. Goeldner, C. Hirth, P. Axersen, I. Silman, and J. Sussman, Quaternary ligand binding to aromatic residues in the active-site gorge of acetylcholinesterase, *Proc. Natl. Acad. Sci. USA* **90,** 9031–9035 (1993).
10. Y. Bourne, P. Taylor, and P. Marchot, Acetylcholinesterase inhibition by fasciculin: Crystal structure of the complex, *Cell* **83,** 503–512 (1995).
11. M. L. Raves, M. Harel, Y. P. Pang, I. Silman, A. P. Kozikowski, and J. L. Sussman, Structure of acetylcholinesterase complexes with the nootropic alkaloid (−)-huperzine A, *Nat. Struct. Biol.* **4,** 57–63 (1997).
12. I. Silman, C. B. Millard, A. Ordentlich, H. M. Greenblatt, M. Harel, D. Barak, A. Shafferman, and J. L. Sussman, A preliminary comparison of structural models for catalytic intermediates of acetylcholinesterase, *Chem. Biol. Interact.* **119–120,** 43–52 (1999).
13. C. B. Millard, G. Kryger, A. Ordentlich, M. Harel, M. L. Raves, Y. Segall, D. Barak, A. Shafferman, I. Silman, and J. L. Sussman, Crystal structures of aged phosphonylated acetylcholinesterase: Nerve agent reaction products at the atomic level, *Biochemistry* **38,** 7032–7039 (1999).
14. H. Sugimoto, Y. Imura, Y. Yamanishi, and K. Yamatsu, Synthesis and structure–activity relationships of acetylcholinesterase inhibitors—1-benzyl-4-[(5,6-dimethoxy-1-oxoindan-2-yl)methyl]piperidine and related compounds, *J. Med. Chem.* **38,** 4841–4829 (1995).
15. D. H. Cheng, H. Ren, and X. C. Tang, Huperzine A, a novel promising acetyl-cholinesterase inhibitor, *Neuroreport* **8,** 97–101 (1996).
16. M. R. Del Giudice, A. Borioni, C. Mustazza, F. Gatta, A. Meneguz, and M. T. Volpe, Synthesis and cholinesterase inhibitory activity of 6-, 7-methoxy-(and hydroxy-) tacrine derivatives, *Farmaco* **51,** 693–698 (1996).
17. G. A. Morris and R. Freeman, Selective excitation in Fourier transform nuclear magnetic resonance, *J. Magn. Reson.* **29,** 433–462 (1978).
18. H. Geen, X.-L. Wu, P. Xu, J. Friedrich, and R. Freeman, Selective excitation at two arbitrary frequencies. The double-DANTE sequence, *J. Magn. Reson.* **81,** 646–652 (1989).
19. R. Freeman, H. D. W. Hill, B. L. Tomlinson, and L. D. Hall, Dipolar contribution to NMR spin–lattice relaxation of protons, *J. Chem. Phys.* **61,** 4466–4473 (1974).
20. H. Sigel and N. A. Corfù, The assisted self-association of ATP4- by a poly(amino acid) [poly(Lys)] and its significance for cell organelles that contain high concentrations of nucleotides, *Eur. J. Biochem.* **240,** 508–517, (1996).
21. L. D. Hall and H. D. W. Hill, Spin–lattice relaxation of protons. A general, quantitative evaluation of contributions from the intramolecular dipole–dipole mechanism, *J. Am. Chem. Soc.* **98,** 1269–1270 (1976).
22. G. Valensin, T. Kushnir, and G. Navon, Selective and nonselective proton spin–lattice relaxation studies of enzyme–substrate interactions, *J. Magn. Reson.* **46,** 23–29 (1982).
23. E. Gaggelli, G. Valensin, T. Kushnir, and G. Navon, Determination of absolute values of dipolar cross-relaxation rates for ligands bound to macromolecules using double-selective T_1, *Magn. Reson. Chem.* **30,** 461–465 (1992).
24. E. Gaggelli, N. Gaggelli, A. Maccotta, and G. Valensin, ^{1}H NMR relaxation investigation of the interaction of vinblastine with tubulin, *J. Magn. Reson. B* **104,** 89–94 (1994).
25. G. Veglia, M. Delfini, M. R. Del Giudice, E. Gaggelli, and G. Valensin, ^{1}H NMR studies on the interaction of β-carboline derivatives with human serum albumin, *J. Magn. Reson.* **130,** 281–286 (1998).
26. G. Valensin, E. Gaggelli, and P. E. Valensin, Proton relaxation investigations of drugs bound to macromolecular receptors, *in* "NMR Spectroscopy in Drug Research" (J. W. Jaroszewski, K. Schaumburg, and H. Kofod, Eds.), pp. 409–422, Munksgaard, Copenaghen (1988).